



Research article

ECG compression with Douglas-Peucker algorithm and fractal interpolation

HichemGuedri^{1,*}, Abdullah Bajahzar² and Hafedh Belmabrouk³

¹ Electronics and Microelectronics Laboratory, Physics Department, Faculty of Sciences, Monastir University, Monastir 5019, Tunisia.

² Department of Computer Science and Information, College of Science, Majmaah University, Zulfi 11932, Saudi Arabia.

³ Department of Physics, College of Science Zulfi, Majmaah University, Zulfi 11932, Saudi Arabia.

* **Correspondence:** Email: Hichem.Guedri@fsm.rnu.tn; Tel: +21697456167.

Abstract: In this paper, we propose a new ECG compression method using the fractal technique. The proposed approaches utilize the fact that ECG signals are a fractal curve. This algorithm consists of three steps: First, the original ECG signals are processed and they are converted into a 2-D array. Second, the Douglas-Peucker algorithm (DP) is used to detect critical points (compression phase). Finally, we used the fractal interpolation and the Iterated Function System (IFS) to generate missing points (decompression phase). The proposed (suggested) methodology is tested for different records selected from PhysioNet Database. The obtained results showed that the proposed method has various compression ratios and converges to a high value. The average compression ratios are between 3.19 and 27.58, and also, with a relatively low percentage error (PRD), if we compare it to other methods. Results depict also that the ECG signal can adequately retain its detailed structure when the PSNR exceeds 40 dB.

Keywords: electrocardiogram (ECG); compression method; Douglas-Peucker algorithm (DP); fractal interpolation; Iterated Function System (IFS)

1. Introduction

The electrocardiogram or ECG is a major examination in cardiology [1,2]; it is used to make a precise diagnosis, particularly arrhythmias, infarction or pericarditis [3,4]. An electrocardiogram

(ECG) records the heart's electrical activity [1,2]. Electrical stimulation of a heart muscle cell results in the appearance of Electrical and mechanical activities that can be recorded, specifically; the ECG studies the electrical activity of the atria and ventricles [3,4]. They use electrodes, which are placed on the different areas, such as on the patient's chest, wrists and ankles, the recorded electrical activity can be done away from the heart [5,6]. The electrodes record either a difference in electric current between two points (bipolar leads with two electrodes) or the electric current directly through a single electrode (unipolar leads). For each lead, an ECG trace is recorded, 12 leads are conventionally recorded on the ECG trace and can be extended to 18 leads under certain circumstances. Indeed, the recorded ECG signals number is huge, which poses a big problem in terms of storage space (either in servers or in storage devices) and transfer time between cardiologists or between a cardiologist and his patient [7,8].

In this study, we were interested in improving the ECG signal compression, to limit the storage space required on the server and the transfer times of these signals [9–13]. In this regard, we have proposed the fractal method for the ECG signals compression and decompression. In order to achieve this aim, the DP method used to compress data signals [14–19]. Then, the fractal interpolation and the IFS algorithm were implemented to rebuild this signal [23–33].

This document is organized as follows; Section 2 summarizes the work related to the signals and images interpolated by fractal interpolation. Subsequently, the proposed methods steps are described in Section 3. Section 4 presents the ECG signal and its characteristics. In Section 5, the DP algorithm is detailed. Then, Section 6 presents the mathematical approach applied in fractal interpolation. Section 7 described the obtained results and Section 6 these are discussed. Finally, Section 8 details the conclusions.

2. Related works

Many of the previous works have employed to compress the electrocardiogram (ECG) records. Ranjeet et al. [10] have proposed three techniques for the compression of electrocardiogram (ECG) signal. The first technique depends on the Discrete Wavelet Transform (DWT) method. The second technique used Fast Fourier Transform (FFT) method. The last technique is based on Discrete Cosine Transform (DCT) method. Abo-Zahhad et al. [11] suggested a strategy for maximum reduction in the data volume of ECG signals while ensuring the reconstruction quality. Their proposed method is based on the optimal selection of wavelet filters and threshold levels in different sub-bands. They begin by segmenting the ECG signal into frames, these frames are broken down into m sub-bands using optimized wavelet filters. They removed any resulting wavelet coefficients that have absolute values less than the specified threshold levels, the remaining coefficients are encoded with a modified version of the serial length encoding scheme. Before encoding, they adjust the threshold levels optimally to achieve the preset compression rate and signal quality. Abo-Zahhad et al. [12] have introduced a method to compress the electrocardiogram (ECG) signals. Their method is based on QRS detection, estimation and thresholding of 2D DWT coefficients. In the preprocessed phase, they detected the QRS-complex. Then, they estimated the difference between the preprocessed ECG signal and the estimated QRS-complex waveform. Later, they cutted and aligned the error signal to form a 2-D matrix which will be transformed into wavelets. The 2-D matrix gave wavelet coefficients as results, the previous are segmented into categories by two grouping techniques, and they threshold it (The threshold level of each group of coefficients is calculated based on the entropy

of the coefficients). The resulted threshold DWT coefficients are coded by the Abo-Zahhad coding technique [13]. Rebollo-Neira [36] has introduced a fast wavelet transform for compression of ECG signals. This technique falls within the transform lossy compression category. Her proposed method is divided into major three steps: 1) Approximation Step 2) Quantization Step 3) Organization and Storage Step.

3. Material and methods

3.1. Block diagram of the proposed method

Figure 1 illustrates the block diagram of the proposed methodology for compression and decompression ECG signal using a fractal technique. The suggested method has three main steps. First, reading the file containing the ECG signals and detecting the curve shapes. Then, detecting the critical points using the Douglas-Peucker algorithm according to the different tolerance values ϵ . eventually, we are presenting the fractal interpolation and IFS method. This step is divided into two sub-parts; we begin by calculating the coefficient values a_n, c_n, d_n, f_n and e_n , aiming to determine the transfer equation W_n . In the second sub-part, we use the transfer equation to generate the new points (see Figure 1).

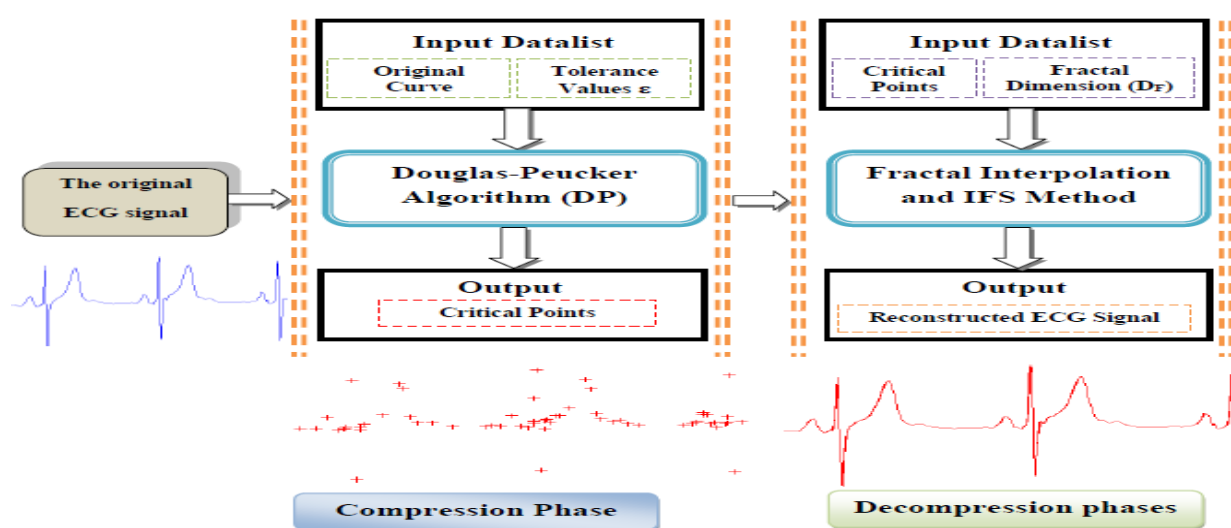


Figure 1. Block diagram of the proposed methodology.

3.2. Electrocardiogram signal (ECG)

The electrocardiogram (ECG) is used to see the electrical activity of the heart, as it produces small electrical impulses. This simple, non-invasive measurement make easy to identify different heart conditions, as it is used to assess symptoms that can be attributed to heart problems (chest pain, breathing problems, tachycardia or a heart rhythm disorder or leg swelling). Figure 2 shows the different parts of the normal ECG signal, the previous is divided into three main parts (atria systole, atria diastole and ventricular systole, and ventricular systole). It is also characterized by five peaks and valleys marked by the letters P, Q, R, S, T [5–8].

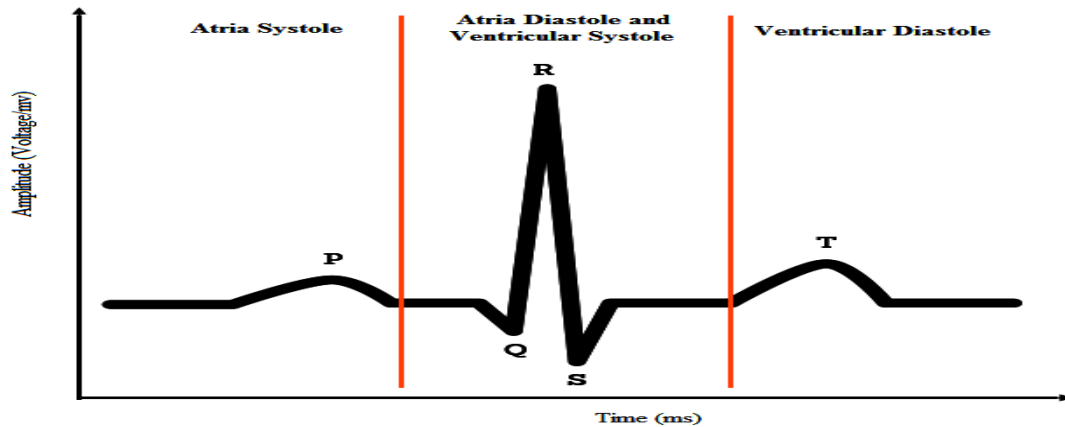


Figure 2. Typical ECG signal.

Indeed, the P wave represents the first stage of the cycle, where the atria systole allowing blood to pass through the auriculo-ventricular valves to the ventricles. The QRS complex symbolizes both the ventricular systole (allowing the blood ejection towards the arteries) in particular by the peak in R, simultaneously; the atria diastole causes the filling of these while waiting for a new cycle. The T wave presents the ventricular diastole following their systole phase [7,8].

3.3. Identification of critical points

The line simplification algorithm is used to simplify lines and polygons. It is employed in order to reduce the complexity entities retains the critical points that describe the overall line shape (while retaining the inherent character and shape) and removes all other points. There are several simplification algorithms that will generate slightly different results, such as the Douglas-Peucker algorithm (DP), the Area-Based algorithm, the Visvalingam algorithm, etc [14–19]. In the same context, many studies control the deviation between the resulting spline and the vertices of the original plot for different simplification algorithms. Especially we cited the McMaster study [20], which showed that mathematically and conceptually, the Douglas-Peucker algorithm was superior to other algorithms. It is the same for White study [21] which uses Marino work [22] with three types of simplification algorithms. [21] He showed that the results obtained by the Douglas-Peucker algorithm give the best examples of lines compared to the original lines with an 86% efficacy rate at all the tests. The Douglas-Peucker algorithm works recursively. The algorithm 1 takes as input a polygon or a curve (ordered sequence of points on plane, $p = (p_1, p_2, \dots, p_n)$,) and a tolerance ϵ . Algorithm 1 illustrates the dynamics and the main steps of the algorithm, and Figure 3(a)–(e) shows the recursively generated tasks of a segmentation example (see Figure 3(a)). In the initial step, the first and last points of the curve are connected by an H line (see Figure 3(b),(c)). Most of the calculation work is done in Steps 2 and 3 (see Figure 3(d),(e))all the curve points are traversed and the maximum perpendicular distance is calculated with the line H, the farthest point of the segment is selected. If the maximum perpendicular distance is less than the tolerance ϵ , all points are deleted and the algorithm ends. If it is greater, the curve is divided into two subparts (the first point to the maximum distant point, and from the maximum distant point to the end point). We recursively redo the algorithm on these two sub-parts of the curve [14–19].

Algorithm 1. Douglas-Peucker algorithm.

 Algorithm 1. Douglas-Peucker algorithm (C, ϵ , Startpoint, Endpoint)

 %% Curve C (an ordered set of points (P_1, \dots, P_n)) (Figure 3(a))

 %% Threshold value ϵ ($\epsilon > 0$)

 %% Startpoint = $P_1 (x_1, y_1)$ and Endpoint = $P_n (x_n, y_n)$.

1. $I_{\max} = 0$ %% maximum point coordinate initialization
2. $Dist_{\max} = 0$ %% maximum orthogonal distance initialization
3. Connect start and end point (P_1 to P_n) with LineH (Figure 3(b),(c))
4. calculate the perpendicular distance of all the points on the line (Figure 3(d))

For $i = 2$ **to** length (C)-1 **do**

 Dist = computeDist (P_i , Startpoint, Endpoint)

If dist > Dmax **then**

 I_{max} = I, Dist_{max} = dist

End If
End For
If Dmax > ϵ **then**

 C1 = curve ($P_1, P_{I_{\max}}$) } (Figure 3(e))

 C2 = curve ($P_{I_{\max}}, P_n$) }

 Result = Douglas-Peucker algorithm (C1, ϵ , P_1 , $P_{I_{\max}}$)

 Result = Douglas-Peucker algorithm (C2, ϵ , $P_{I_{\max}}$, P_n)

Else

Result = (Startpoint, Endpoint)

End if

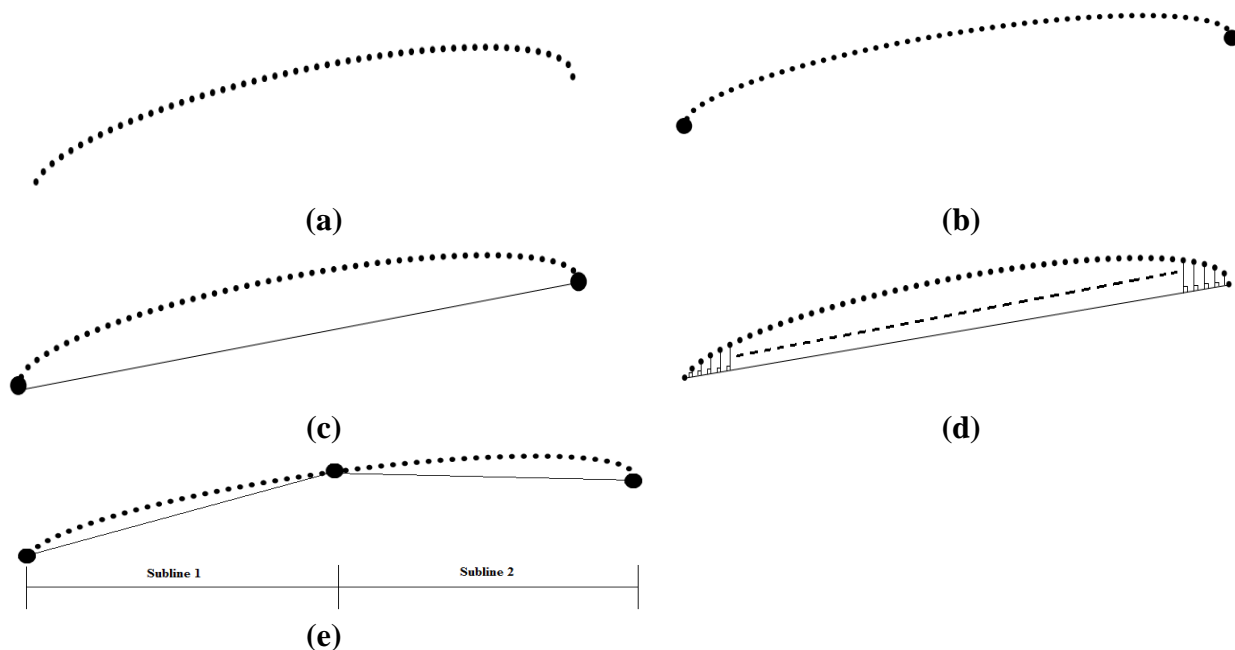


Figure 3. Douglas-Peucker algorithm, (a) Segmentation example, (b) The start and end points, (c) Connect start and end points, (d) Calculate the perpendicular distances, (e) Two subparts of curve.

3.4. Fractals object construction

We call fractal of a geometric object which by zooming on one (or more) part(s), we get the same as the initial object [23–27].

3.4.1. The Iterated Functions System (IFS)

Definition 1. An Iterated Functions System (IFS) is a pair data $(Y, (W_n)_{1 \leq n \leq N})$ with Y a complete metric space and for all $i \in \llbracket 1, N \rrbracket$, the application $W_i: Y \rightarrow Y$ being a contracting party [23–25].

Definition 2. Let $(Y, (W_n)_{1 \leq n \leq N})$ is an IFS. We defined by the following Eq (1):

$$\begin{aligned} W_i: Y &\rightarrow Y \\ A &\rightarrow \bigcup_{n=1}^N W_n(A) \end{aligned} \quad (1)$$

Let (\mathbb{I}, d_H) be a complete metric space. In the following, we will therefore be satisfied with treating the IFS case with the associated set being K .

Definition 3. A set $F \in \mathbb{I}$ such that $W(F) = F$ is called an SFI attractor [26,27].

3.4.2. Fractal interpolation

We therefore consider a subdivision (x_0, x_1, \dots, x_N) and $y_i = f(x_i)$, with $(x_0 < x_1 \ll x_N)$. We set $I = [x_0, x_n]$ the segment on which we will interpolate the function [27–30].

Let us assume, for $n \in \llbracket 1, N \rrbracket$, the segment $I_n = [x_{n-1}, x_n]$ and the affine application Eq (2):

$$\begin{aligned} L_n: I &\rightarrow I_n \\ x &\rightarrow a_n x + e_n \end{aligned} \quad (2)$$

With the parameters a_n and e_n fixed by the following Eq (3):

$$L_n(x_0) = x_{n-1}; L_n(x_N) = x_n \quad (3)$$

The purpose is to “zoom in” on the x -axis. We must now define the operation that takes place when zooming on the y -axis.

We define the set $C = \{f \in C^0(I), f(x_0) = y_0, f(x_N) = y_N\}$ provided with the norm $\| \cdot \|_\infty$.

Let the following Eq (4) [27–30]:

$$\begin{aligned} F_n: \mathbb{R}^2 &\rightarrow \mathbb{R} \\ (x, y) &\rightarrow c_n x + d_n y + f_n \end{aligned} \quad (4)$$

With $F_n(x_0, y_0) = y_{n-1}$ and $F_n(x_N, y_N) = y_n$ and the d_n being free parameters in $]-1, 1[$. Finally we define the operator Eq (5) [23–30]:

$$\begin{aligned} T: C &\rightarrow C \\ f &\rightarrow Tf \end{aligned} \quad (5)$$

Defines for $x \in I_n$ by $Tf(x) = F_n(L_n^{-1}(x), f \circ L_n^{-1}(x))$.

Corollary: T admits a unique fixed point $f \in C$ with $f(L_n(x)) = F_n(x, f(x))$.

Proposition: The f graph is the IFS attractor $(I \times \mathbb{R}, (W_n)_{1 \leq n \leq N})$ with the following Eq (6) [25–33]:

$$W_n(x, y) = \begin{pmatrix} a_n & 0 \\ c_n & d_n \end{pmatrix} \begin{pmatrix} x \\ y \end{pmatrix} + \begin{pmatrix} e_n \\ f_n \end{pmatrix} = \begin{pmatrix} L_n(x) \\ F_n(x, y) \end{pmatrix} \quad (6)$$

Coefficients equations:

$$\begin{aligned} a_n &= \frac{x_n - x_{n-1}}{x_N - x_1} \\ e_n &= \frac{x_N x_{n-1} - x_1 x_n}{x_N - x_1} \\ c_n &= \frac{y_n - y_{n-1}}{x_N - x_1} - d_n * \frac{y_N - y_1}{x_N - x_1} \\ f_n &= \frac{x_N y_{n-1} - x_1 y_n}{x_N - x_1} - d_n * \frac{x_N y_1 - x_1 y_N}{x_N - x_1} \\ d_n &= (N - 1)^{D_F - 2} \end{aligned}$$

With N is the total number of data points and D_F is the fractal dimension. Based on the study by Marie [34] and Namazi and Kulish [35] the fractal dimension of the ECG signals can be determined.

3.4.3. Algorithm

Let N points $\{P_n = (P_1, \dots, P_N)\} \in E$ and N transformation $W_n = (W_1, \dots, W_N)$. We take a point $P_1 \in E$ and we set all the new points $\hat{P}_2 = W_n(P_1)$. Then we repeat [30–33]. We thus obtain a continuation $(P_i)_i$. We set F all these points, as shown in Figure 4:

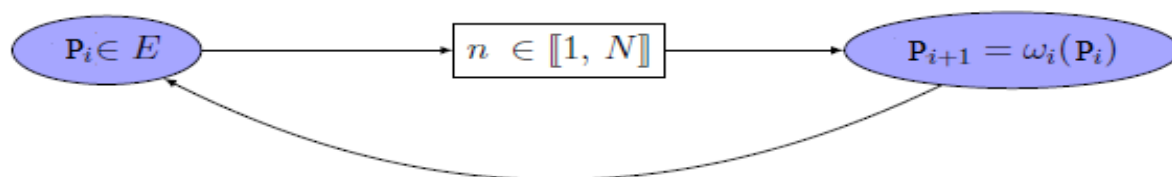


Figure 4. Algorithm IFS.

3.4.4. Performance evaluation

In this section, we examine the compression performance and the effect of varying parameters on the reconstructed signal quality. At this stage we introduce the PRD, CR and PSNR measurements to evaluate the results of the proposed procedure [12,36–40].

We assessed the compression performance using the Compression Ratio (CR) as is given by the following Eq (7) [12,36–40]:

$$CR = \frac{\text{Size of the uncompressed signal}}{\text{Size of the compressed signal}} \quad (7)$$

We evaluated the recovered signal quality by PRD value. The PRD definition is given by the following Eq (8) [12,36–40]:

$$PRD = \sqrt{\frac{\sum_{n=1}^N (x(n) - \hat{x}(n))^2}{\sum_{n=1}^N x(n)^2}} \times 100 \quad (8)$$

The peak signal-to-noise ratio PSNR will be calculated using Eq (9) as follows:

$$PSNR = 10 \log_{10} \left(\frac{M^2}{MSE} \right) = 10 \log_{10} \left(\frac{M^2}{\sqrt{\frac{1}{N} \sum_{n=1}^N (x(n) - \hat{x}(n))^2}} \right) \quad (9)$$

where $x(n)$ is the original signals, $\hat{x}(n)$ is the rebuilt signals, the constant M is the difference between the maximal value and the minimal value of the used test data, (MSE) is the mean square error and N is the test data length.

4. Results

The numerical simulations and the obtained results are performed using Windows 7 64-bit on an Intel Intel Pentium B960 CPU @ 2.20 GHz with 4 GB of memory. We implemented the Douglas-Peucker methods and fractal interpolation using MATLAB R2017a. To verify the correctness and effectiveness of the suggested method, we used real ECG signals on a publicly available PhysioNet database [52,53]. Each ECG signal in this dataset has at least two trajectories with 5000 points. The process of the proposed methodology is divided into three major phases. The first step is to read the ECG signal, the second is the compression phase, in which we use the PD algorithm, and the final phase is the reconstruction phase (decompression phase).

4.1. The electrocardiogram signals read (ECG)

The ECG signals used from PhysioNet database are MAT type files, in this spirit, we employed the 'load' instruction, which allows us to load the variables file in Matlab, as shown below:

`S = load (filename, '-mat' % S is a structure array.`

The frequency margin for normal ECG signals is between 0.05 and 100 Hz, and its dynamic amplitude range from 1 to 10 mV.

In the normal state of the heart, the normal heart rate is between 60 and 100 beats per minute, the time range for each ECG signal interval is as follows [8,52,54]:

- For the P-R interval, it is between 0.12 and 0.2 seconds,
- For the QRS interval, its time margin is between 0.04 and 0.12 seconds.
- For Q-T interval, the time margin is less than 0.42 seconds.

4.2. DP algorithm result

In this section, the validity of the proposed DP algorithm is applied to the real trajectory ECG

signals set. The proposed DP algorithm is used to compress the ECG signal trajectories. Figure 5 shows the original and compressed trajectories for different threshold values \mathcal{E} . Figure 5(a) is the original trajectory of the ECG signal. The Figure 4(b)–(h) are respectively the compressed trajectories for the threshold values \mathcal{E} equal to 0.1×10^{-6} , 0.4×10^{-6} , 0.7×10^{-6} , 1×10^{-6} , 1.5×10^{-6} , 2.5×10^{-6} and 4.5×10^{-6} , respectively. During this time, Figure 5(b)–(h) shows the point data before and after compression (red points represent the original trajectory and blue points represent the compressed trajectories). We can note from Figure 6 that the data volume is reduced under this algorithm, while keeping the original topological signal.

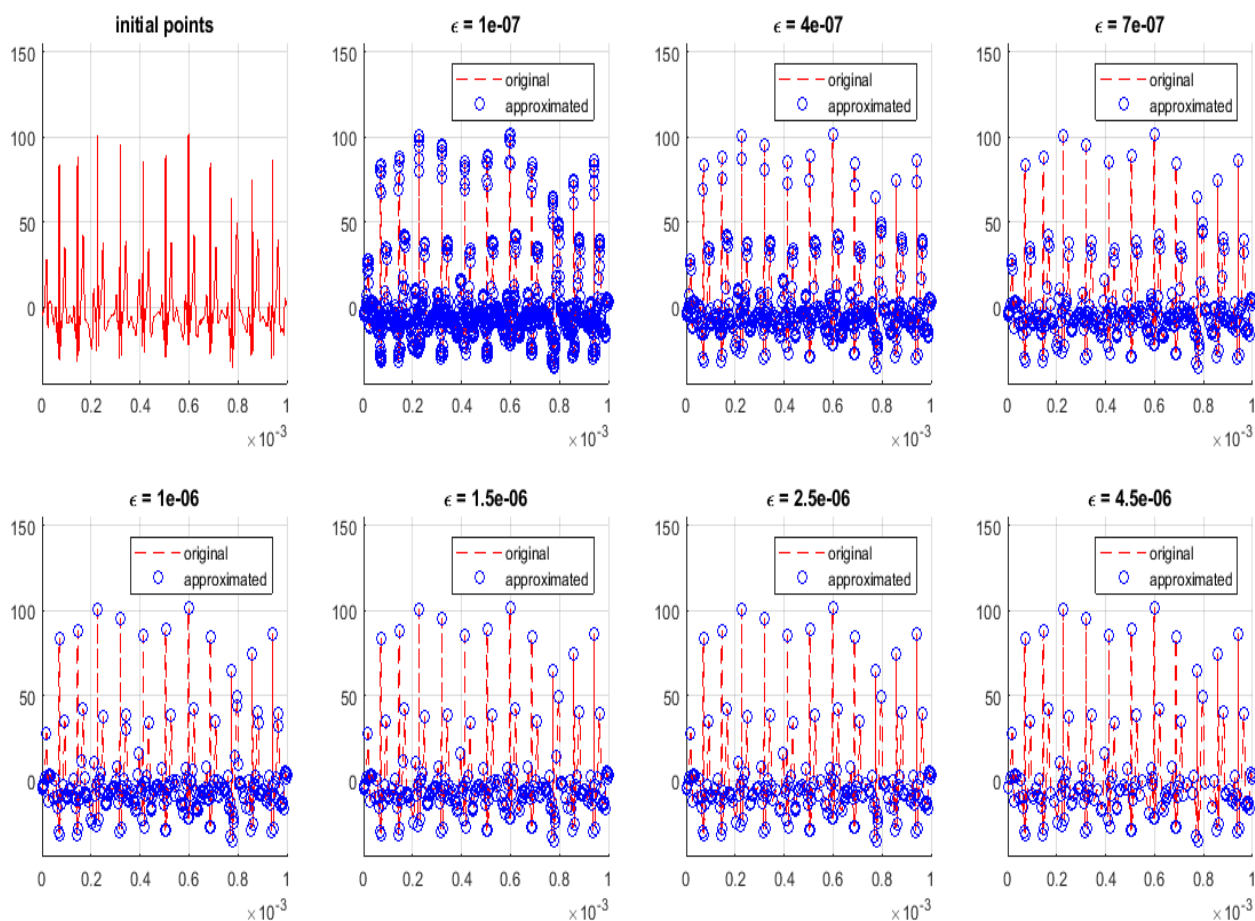


Figure 5. DP algorithm results, (a) Original trajectory of the ECG signal, (b) Compressed trajectories for $\mathcal{E} = 0.1 \times 10^{-6}$, (c) Compressed trajectories for $\mathcal{E} = 0.4 \times 10^{-6}$, (d) Compressed trajectories for $\mathcal{E} = 0.7 \times 10^{-6}$, (e) Compressed trajectories for $\mathcal{E} = 1 \times 10^{-6}$, (f) Compressed trajectories for $\mathcal{E} = 1.5 \times 10^{-6}$, (g) Compressed trajectories for $\mathcal{E} = 2.5 \times 10^{-6}$, (h) Compressed trajectories for $\mathcal{E} = 4.5 \times 10^{-6}$.

The Compression Ratio values (CR) for the reconstructed signal obtained from ten tested signals for different threshold values \mathcal{E} (0.1×10^{-6} , 0.4×10^{-6} , 0.7×10^{-6} , 1×10^{-6} , 1.5×10^{-6} , 2.5×10^{-6} and 4.5×10^{-6}) are listed in Table 1. The numerical experiments are implemented and a DP algorithm simulation on ten different classes of ECG signals.

Table1. The Compression Ratio values (CR).

\mathcal{E}	0.1×10^{-6}	0.4×10^{-6}	0.7×10^{-6}	1×10^{-6}	1.5×10^{-6}	2.5×10^{-6}	4.5×10^{-6}
Person_01/rec_1	3.531	7.764	12.077	16.181	19.841	25	34.722
Person_02/rec_1	3.073	7.072	11.389	14.326	16.077	19.607	25
Person_03/rec_1	3.291	7.728	13.054	15.7234	19.305	22.123	25.125
Person_04/rec_1	3.168	7.385	12.019	15.480	18.315	21.367	25
Person_05/rec_1	3.084	7.173	11.627	13.927	16.949	21.008	27.472
Person_06/rec_1	3.146	7.610	12.077	14.705	16.393	20.408	29.762
Person_07/rec_1	3.037	6.877	10.822	14.005	16.949	19.920	26.738
Person_08/rec_1	3.148	7.396	11.820	14.492	16.722	21.834	26.881
Person_09/rec_1	3.113	7.173	11.261	14.204	16.02	21.008	29.239
Person_10/rec_1	3.340	7.740	12.5	15.974	19.455	21.459	25.906
Average	3.19	7.39	11.86	14.90	17.60	21.37	27.58

The results in Table 1 show that:

-The average compression ratios are between 3.19 and 27.58.

-It can be seen from Table 1 that the average compression ratio values are 3.19, 7.39, 11.86, 14.90, 17.60, 21.37, 27.58 for the threshold values $\mathcal{E} = 0.1 \times 10^{-6}$, 0.4×10^{-6} , 0.7×10^{-6} , 1×10^{-6} , 1.5×10^{-6} , 2.5×10^{-6} and 4.5×10^{-6} , respectively.

-In addition, the smaller the threshold values \mathcal{E} , the lower the average compression ratios are, e.g., for $\mathcal{E} = 0.1 \times 10^{-6}$ the average compression ratio value is 3.19, vice versa, the larger the threshold values \mathcal{E} , the higher the compression ratio are, as shown in Table 1, for $\mathcal{E} = 4.5 \times 10^{-6}$, the average compression ratio value approximates to 27.5.

4.3. IFS results

Figure 7 shows the results of the suggested method for a selected record from the PhysioNet database Person_01/rec_1, for different threshold values \mathcal{E} and for an iteration number $K = 500$. Figure 6 evaluation show that the reconstructed ECG signal retained the most information of the original signal (red points represent the original trajectory and blue points represent the reconstructed trajectories).

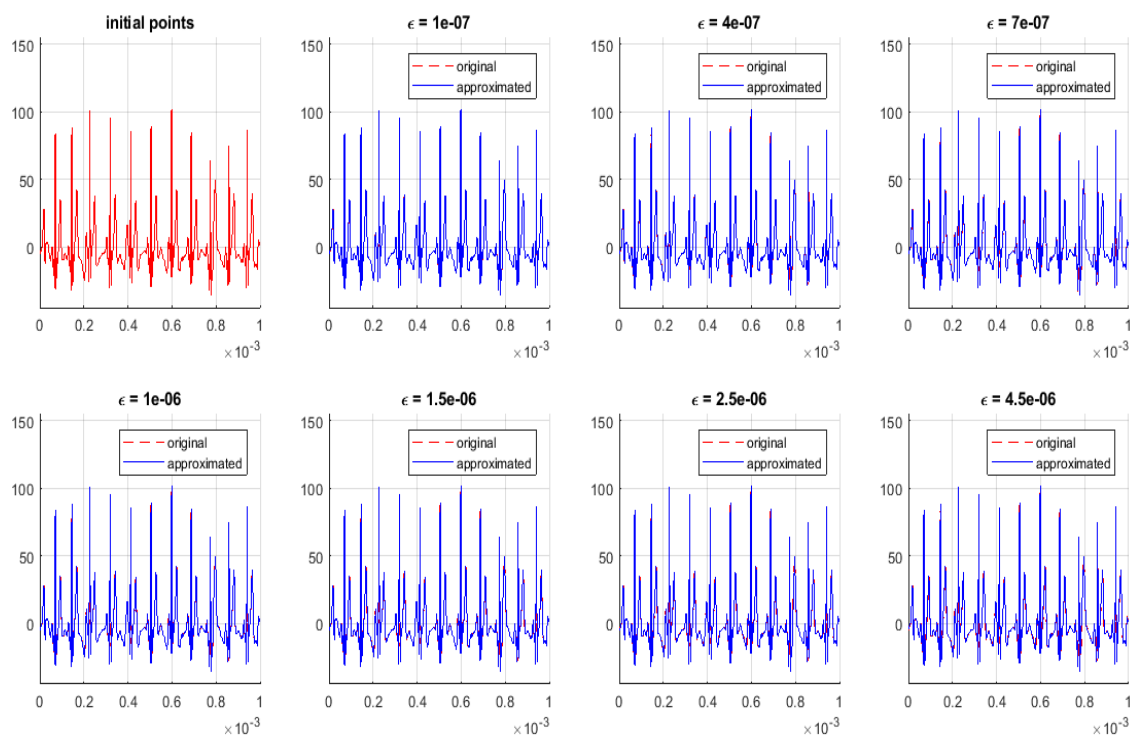


Figure 6. IFS result for iteration number $k = 500$.

Figure 7 shows the error measurement for various threshold values \mathcal{E} and for an iteration number $K = 500$. This measurement reflects the distance between the original ECG signal and the reconstructed ECG signal. The error calculation is based on the following Eq (10):

$$E(n) = x(n) - \hat{x}(n), \quad n = 1, \dots, N \quad (10)$$

where $E(n)$ is the error signal, $x(n)$ is the original signals, $\hat{x}(n)$ is the reconstructed signals and N is the signal length.

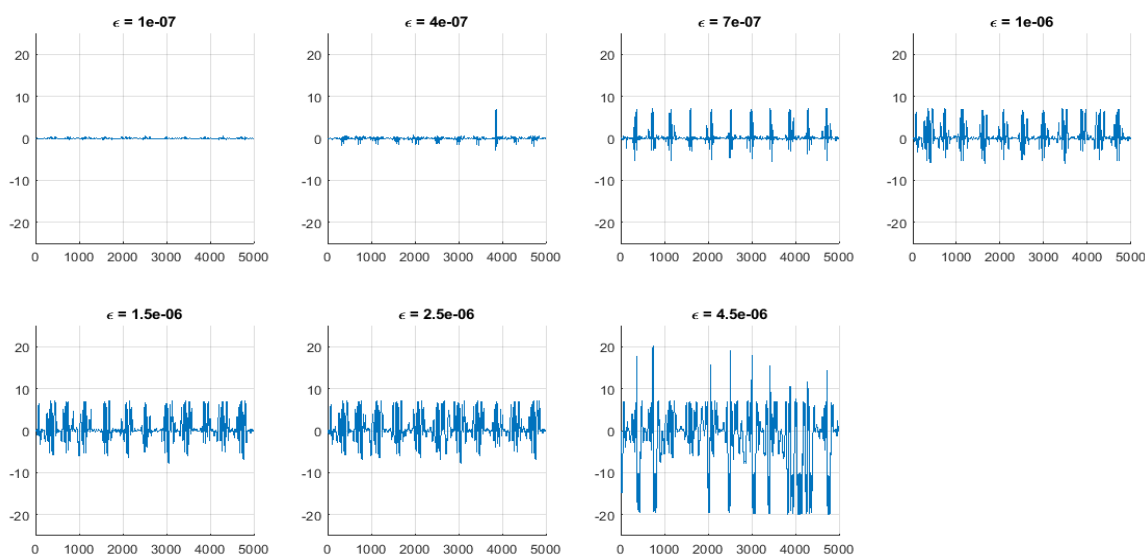


Figure 7. Signal error at various threshold values \mathcal{E} .

From the obtained result, we can see that the more the threshold values ϵ the more tangible the margin of error. Contrariwise, the lower the threshold values ϵ , the smaller the margin of error, as a greater signal precision, as shown in Figure 7. The detailed structure of the error measurement of various threshold values ϵ and for an iteration number $K = 500$ is shown in Figure 7. The PSNR value with the same criteria is given in Table 2. It is obviously seen that, with more interpolation points, ECG signal detailed structure emerges, exhibiting a closest to the original signal.

Table 2. PSNR value at various threshold values ϵ .

ϵ	0.1×10^{-6}	0.4×10^{-6}	0.7×10^{-6}	1×10^{-6}	1.5×10^{-6}	2.5×10^{-6}	4.5×10^{-6}
Person_01/rec_1	55.50	48.73	45.94	42.88	41.97	41.64	38.87
Person_02/rec_1	53.17	47.83	44.06	42.69	41.47	40.12	38.32
Person_03/rec_1	55.21	50.17	43.38	42.41	40.99	39.82	36.78
Person_04/rec_1	55.24	52.13	44.53	42.88	41.83	40.65	36.37
Person_05/rec_1	51.38	45.59	45.22	42.74	41.26	39.73	36.99
Person_06/rec_1	54.56	48.70	43.34	42.21	40.66	39.98	36.69
Person_07/rec_1	55.29	51.91	43.49	41.53	40.72	38.96	36.87
Person_08/rec_1	54.36	50.05	44.42	42.03	40.86	38.95	36.16
Person_09/rec_1	55.22	51.34	44.88	42.21	40.93	38.50	35.64
Person_10/rec_1	55.23	50.25	44.30	41.89	40.81	38.93	35.73
Average	54.516	49.67	44.356	42.347	41.15	39.728	36.842

According to the test result depicted in Table 2, the lower the threshold values ϵ , the lower the compression ratio, the more data points are retained, and the PSNR increases, which indicates a signal with less than distortion and better quality (e.g., for $\epsilon = 0.1 \times 10^{-6}$ the average PSNR value is 54.516 dB, the average PSNR value is approximately 41.15 dB and 36.842 dB for $\epsilon = 1.5 \times 10^{-6}$ and $\epsilon = 4.5 \times 10^{-6}$, respectively). It can be concluded from the obtained PSNR values in Table 2, the results of the ECG signal curves in Figure 6 and the detailed error structure in Figure 7 that when the PSNR exceeds 40 dB, the geographical characteristics of the ECG signals can be fully retained.

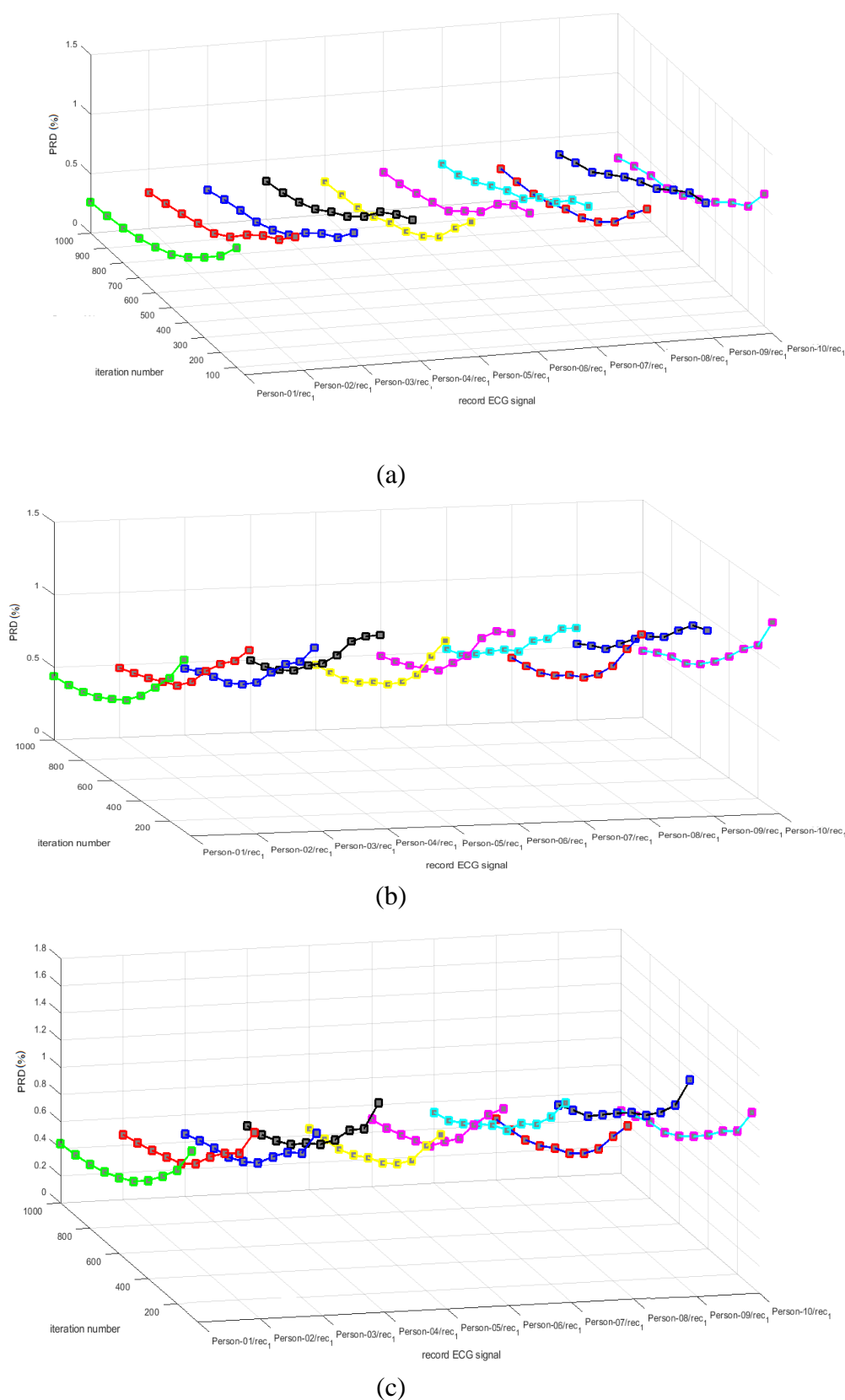


Figure 8. PRD curves for the test ECG records.

Figure 8 shows the PRD curves of the proposed method. Figure 8(a)–(c) and c illustrate the PRD results for three threshold values $\varepsilon 0.1 \times 10^{-6}$, 1×10^{-6} and 4.5×10^{-6} , respectively, and at the

same time, for iteration numbers between 100 and 1000. This digital test aims to compare the ECG signals obtained with the original signals. It was noted that the mean PRD value in range from 0.28 to 1.1%, for high values of ϵ , they are reported for the mean PRD value in the range 0.54 to 1.62%, and for mean values of ϵ the mean PRD value is between 0.46 and 1.28%. This leads us to conclude that the good reconstruction on is made on the basis of the low CR values, and therefore, for threshold values ϵ less than 1×10^{-6} . As already noted if the iterations number K increases, the PRD value is deprived, vice versa, the smaller the K , the higher the PRD value are, as shown in Figure 8.

5. Discussion

The numerical results obtained from this study are compared with the previous compression methods available in the literature. To evaluate the performance of the proposed method with existing published works in the similar area [12,36–51], two parameters are employed: the first is the compression ratio (CR) and the second is the Percent Root-Mean Square difference (PRD), as outline in Table 3.

Table 3. Comparison with previous study.

No.	Year	Study	CR	PRD (%)
		Proposed method	3.19–27.58	0.28–1.6
1	2012	Abo-Zahhad et al. [12]	8.2–38.6	0.66–1.6
2	2019	Rebollo-Neira [36]	23.17	0.53
3	2016	Garg et al. [37]	1:20	1.26–2.51
4	2009	Mohammadpour et al. [38]	8–24	0.52–2.8
5	2005	Moazami-Goudarzi et al. [39]	8–30	2–6.7
6	2006	Chou et al. [40]	21.6–24.0	1.81–16.44
7	2017	Kumar et al. [41]	9.02	3.72
8	2014	Kumar et al. [42]	Proposed + DCT 47.83 Proposed + DWT 15.68	10.52 10.38
9		Ranjeet et al. [43]	65	1.44–24.12
10	2021	Kumar et al. [44]	Arrhythmia 43.52 Ompression 42.80	2.52 2.40
11	2016	RajarshiGupta[45]	mitdb, 8 bit (Bit rate Control) 50.74 mitdb, 8 bit (Error Control) 9.48	16.22 4.13
12	2018	Liu et al. [46]	10–120	10.04
13	2017	Liu et al. [47]	1–100	0.2–1.1
14	2018	Mukhopadhyay et al. [48]	63.93	8.09
15	2017	Peng et al. [49]	6.15–27.45	4.15–10.21
16	2017	Wanget al. [50]	106.45	8.00
17	2018	Yildirimet al. [51]	32.25	2.73

It is clear that the proposed algorithm has an acceptable CR value with a very low PRD, which implies that the proposed compression method is suitable for ECG signals. Table 3 depicts that the PRD rates are lower in the proposed study compared to other studies in the literature. The CR rate is

lower compared to some other methods, but at an acceptable level. Therefore, the ECG signals were reconstructed without significant data loss compared to the original data.

For ECG signals, fractal interpolation can produce more data points than initially observed; therefore the reconstructed signals have more natural and real details. Thus, the percent error can be reduced.

The larger the threshold value ϵ , the more reduction the data is, and the higher the compression rate. On the other hand, the error is high in the signals reconstructed, so reconstructing the system leads to higher distortion; conversely, the smaller the threshold values ϵ , the more reduced reduction the data are, and the smaller the compression ratio. As a result, the ECG signals reconstructed with low error and less distortion will be closer to the original data.

Moreover, the proposed method retains the critical points after compression. Compared to previous works which are summarized in Table 3, the proposed method can directly decompress the ECG signal by using affine transformation to add data points. Then, it can improve point-to-point simulation without parameter extraction or signal transformation. Since on the one hand the fractal interpolation is a complex formulation of affine transformation with certain linear functions, inasmuch, the ECG signals are regarded as a complex and irregular curve, we conclude that when the curve is within these type-curves, the fractal technique can better express the real undulation and natural attributes of the curve. Therefore, it is expected that the suggested method is more powerful than traditional techniques.

On the other hand, the result shows that the proposed approach provides the best reconstruction quality as reported in Table 2 as well as in Figures 6 and 8. Furthermore, the proposed method is easily used in practice for remote healthcare, data storage system in healthcare, etc.

The disadvantage of the proposed method is that the decompression phase requires very high computing power. However, this disadvantage can be eliminated using the Supercomputer or the DSP.

6. Conclusions

In this paper, we proposed an ECG compression method using the fractal technique. This approach exploits the fact that ECG signals are a fractal curve. Several algorithms were integrated, including those for processing the ECG signals and converted it into a 2-D array. The next algorithm, which is described in this work, was the detection of critical points by the Douglas-Peucker algorithm; this algorithm is employed to reduce volume data (data reduction methods). At this point, different pre-set tolerances ϵ are used, and such critical points are used to calculate fractal interpolation functions. The fractal interpolation was adopted to rebuild the ECG signals at every compression rate, and for different iteration numbers between 100 and 1000. The numerical results show that the Douglas-Peucker algorithm has various compression ratios and converges to a high value, its range from 3.19 to 27.58. It should be noted that this algorithm is fast and easy to implement, not only with fast execution, but also acceptable compression ratio. In terms of signal reconstruction competence, the fractal method shows that ECG signals can appropriately retain its detailed structure without significant distortions. Also, it was noted that the main PRD value in the range from 0.2 to 1.6 for different threshold values ϵ (at every compression rate), and, at the same time, for iteration numbers between 100 and 1000. Besides, the obtained result shows that the ECG signal have an average PSNR value between 36 and 55 dB. We can conclude, the ECG signal can adequately retain its detailed structure when the PSNR exceeds 40 dB. Finally, it can be

noted that our proposed algorithm will take less time and therefore it will be less costly and it will provide a reproducible and reliable data.

Our future work will focus on the optimization of the compression performance of ECG signals and on finding solutions for implementing the compression system proposed in programmable circuits such as FPGA, DSP, etc. Moreover, it is intended to the storage phase and the transmission of ECG signals between cardiologists or between a cardiologist and his patient on mobile devices. In a similar vein, it is planned to work more closely with the cardiologist, to evaluate the method and to improve it according to their comments.

Conflict of interest

The authors declare no conflict of interest.

References

1. C. C. Chen, C. W. Chen, C. W. Hsieh, Noise-resistant CECG using novel capacitive electrodes, *Sensors*, **20** (2020), 1–17.
2. J. C. Carrillo-Alarcón, L. A. Morales-Rosales, H. Rodríguez-Ráangel, M. Lobato-Báez, A. Muñoz, I. Algreto-Badillo, A metaheuristic optimization approach for parameter estimation in arrhythmia classification from unbalanced data, *Sensors*, **20** (2020), 1–29.
3. M. Yin, R. Tang, M. Liu, K. Han, X. Lv, Influence of optimization design based on artificial intelligence and internet of things on the electrocardiogram monitoring system, *J. Healthc. Eng.*, **2020** (2020), 1–8.
4. N. Reljin, J. Lazaro, M. B. Hossain, Y. S. Noh, C. H. Cho, K. H Chon, Using the redundant convolutional encoder-decoder to denoise QRS complexes in ECG signals recorded with an armband wearable device, *Sensors*, **20** (2020), 1–15.
5. Q. Shen, H. Gao, Y. Li, Q. Sun, M. Chen, An Open-Access arrhythmia database of wearable electrocardiogram, *J. Med. Biol. Eng.*, **40** (2020), 564–574.
6. M. F. Pérez-Gutiérrez, J. J. Sánchez-Muñoz, M. Erazo-Rodas, A. Guerrero-Curienes, E. Everss, A. Quesada-Dorador, Spectral analysis and mutual information estimation of left and right intracardiac electrograms during ventricular fibrillation, *Sensors*, **20** (2020), 1–20.
7. R. Caulier-Cisterna, M. Sanromán-Junquera, S. Muñoz-Romero, M. Blanco-Velasco, Spatial-temporal signals and clinical indices in electrocardiographic imaging (I): preprocessing and bipolar potentials, *Sensors*, **20** (2020), 1–28.
8. R. Ranjan, V. K. Giri, A unified approach of ECG signal analysis, *Int. J. Soft. Comput. Eng.*, **2** (2012), 5–10.
9. L. Rebollo-Neira, Effective high compression of ECG signals at low level distortion, *Sci. Rep.*, **9** (2019), 1–12.
10. K. Ranjeet, A. Kumar, R. K. Pandey, ECG signal compression using different techniques, In *Unnikrishnan S., Surve S., Bhoir D. (eds) Advances in Computing, Communication and Control. ICAC3 2011. Communications in Computer and Information Science*, Springer, Berlin, Heidelberg, **125** (2011).

11. M. Abo-Zahhad, A. F. Al-Ajlouni, S. M. Ahmed, R. J. Schilling, A new algorithm for the compression of ECG signals based on mother wavelet parameterization and best-threshold levels selection, *Digit. Signal Process.*, **23** (2013), 1002–1011.
12. M. Abo-Zahhad, S. M. Ahmed, A. Zakaria, An efficient technique for compressing ECG signals using QRS detection, estimation, and 2D DWT coefficients thresholding, *Model. Simulat. Eng.*, **2012** (2012), 1–10.
13. M. Abo-Zahhad, B. A. Rajoub, An effective coding technique for the compression of one-dimensional signals using wavelet transforms, *Med. Eng. Phys.*, **24** (2002), 185–199.
14. P. Cebrian, J. C. Moure, GPU-accelerated RDP algorithm for data segmentation, In *Krzyszczanovskaya V. et al. (eds) Computational Science-ICCS 2020. ICCS 2020. Lecture Notes in Computer Science*, Springer, Cham, **12137** (2020).
15. X. Wang, W. Yang, Y. Liu, R. Sun, J. Hu, Segmented Douglas-Peucker algorithm based on the node importance, *KSII Trans. Internet. Inf. Syst.*, **14** (2020), 1562–1578.
16. L. Zhao, G. Shi, A method for simplifying ship trajectory based on improved Douglas-Peucker algorithm, *Ocean. Eng.*, **166** (2018), 37–46.
17. Y. Q. Zhang, G. Y. Shi, S. Li, S. K. Zhang, Vessel trajectory online multi-dimensional simplification algorithm, *J. Navig.*, **73** (2020), 342–363.
18. J. Liu, H. Li, Z. Yang, K. Wu, Y. Liu, R. W. Liu, Adaptive Douglas-Peucker algorithm with automatic thresholding for AIS-Based vessel trajectory compression, *IEEE Access*, **7** (2019), 150677–150692.
19. S. Lakhera, T. Praveena, Visual analysis using modified Ramer-Douglas–Peucker algorithm on time series data, *Int. Res. J. Eng. Technol.*, **07** (2020), 4225–4229.
20. R. B. McMaster, Automated line generalisation, *Cartographica*, **24** (1987), 74–111.
21. White, E. R., Assessment of line-generalization algorithms using characteristic point, *Am. Cartographer*, **12** (1985), 17–27.
22. J. S. Marino, Identification of characteristic points along naturally occurring lines. an empirical study, *Can. cart/Toronto.*, **16** (1979), 70–80.
23. S. Dillon, V. Drakopoulos, On self-affine and self-similar graphs of fractal interpolation functions generated from iterated function systems, *Fract. Anal. Appl. Health Sci. Soc. Sci., Fernando Brambila*, **9** (2017), 187–204.
24. R. A. Al-Jawfi, Approximation of fractal interpolation using artificial neural network, *J. Eng. Appl. Sci.*, **15** (2020), 1337–1340.
25. S. I. Ri, New types of fractal interpolation surfaces, *Chaos Soliton. Fract.*, **119** (2019), 291–297.
26. S. I. Ri, A new nonlinear bivariate fractal interpolation function, *Fractals*, **26** (2018), 1–24.
27. V. Drakopoulos, P. Manousopoulos, On non-tensor product bivariate fractal interpolation surfaces on rectangular grids, *Mathematics*, **8** (2020), 1–19.
28. P. R. Massopust, *Fractal Functions, Fractal Surfaces and Wavelets*, 2nd edition, San Diego: Academic Press, 2016.
29. N. Vijender, A. K. B. Chand, Shape preserving affine fractal interpolation surfaces, *Nonlinear Stud.*, **21**(2014), 175–190.
30. M. A. Navascués, A. K. B. Chand, V. P. Veedu, M. V. Sebastián, Fractal interpolation functions: a short survey, *Appl. Math.*, **5** (2014), 1834–1841.
31. M. F. Barnsley, P. R. Massopust, Bilinear fractal interpolation and box dimension, *J. Approx. Theory*, **192** (2015), 362–378.

32. C. Corda, M. FatehiNia, M. Molaei, Y. Sayyari, Entropy of iterated function systems and their relations with black holes and bohr-like black holes entropies, *Entropy*, **20** (2018), 1–17.
33. H. Y. Wang, J. S. Yu, J. S. Yu, Fractal interpolation functions with variable parameters and their analytical properties, *J. Approx. Theory*, **175** (2013), 1–18.
34. M. Rahman, A. H. M. Z. Karim, A. Al-Mahmud, S. N. Rahman, Detection of abnormality in electrocardiogram (ECG) signals based on Katz's and Higuchi's method under fractal dimensions, *Comput. Biol. Bioinform.*, **4** (2016), 27–36.
35. H. Namazi, V. Kulish, Fractal based analysis of the influence of odorants on heart activity, *Sci. Rep.*, **6** (2016), 1–8.
36. L. Rebollo-Neira, Effective high compression of ECG signals at low level distortion, *Sci. Rep.*, **9** (2019), 1–12
37. A. R. Garg, M. K. Mathur, Use of self organizing map to obtain ECG data templates for its compression and reconstruction, *Int. J. Comput. Appl.*, **137** (2016), 26–33.
38. T. I. Mohammadpour, M. R. K. Mollaei, ECG compression with thresholding of 2-D wavelet transform coefficients and run length coding, *Eur. J. Sci. Res.*, **27** (2009), 248–257.
39. M. Moazami-Goudarzi, A. Taheri, M. Pooyan, Efficient method for ECG compression using two dimensional multiwavelet transform, *Int. J. Inf. Technol.*, **2** (2005), 257–263.
40. H. H. Chou, Y. J. Chen, Y. C. Shiau, T. S. Kuo, An effective and efficient compression algorithm for ECG signals with irregular periods, *IEEE. Trans. Biomed. Eng.*, **53** (2006), 1198–1205.
41. R. Kumar, A. Kumar, G. K. Singh, H. N. Lee, Efficient compression technique based on temporal modelling of ECG signal using principle component analysis, *IET Sci. Meas. Technol.*, **11** (2017), 346–353.
42. R. Kumar, A. Kumar, G. Akhil, A. Singh, S. N. H. Jafri, Computationally efficient method for ECG signal compression based on modified SPIHT technique, *Int. J. Biomed. Eng. Technol.*, **15** (2014), 173–188.
43. K. Ranjeet, A. Kumar, Rajesh K. Pandey, An efficient compression system for ECG signal using QRS periods and CAB technique based on 2D DWT and huffman coding, *Control, Autom., Robot. Embedded Syst. (CARE)*, 2013.
44. R. Kumar, A. R. Verma, B. Gupta, S. Kumar, Dual-tree sparse decomposition of DWT filters for ECG signal compression and HRV analysis, *Augment. Hum. Res.*, **6** (2021), 1–8.
45. R. Gupta, Quality aware compression of electrocardiogram using principal component analysis, *J. Med. Syst.*, **40** (2016), 1–11.
46. J. Liu, F. Chen, D. Wang, Data compression based on stacked RBM-AE model for wireless sensor networks, *Sensors*, **18** (2018), 1–19.
47. T. Y. Liu, K. J. Lin, H. C. Wu, ECG data encryption then compression using singular value decomposition, *IEEE J. Biomed. Health Informat.*, **22** (2018), 707–713.
48. S. K. Mukhopadhyay, M. O. Ahmad, M. N. S. Swamy, An ECG compression algorithm with guaranteed reconstruction quality based on optimum truncation of singular values and ASCII character encoding, *Biomed. Signal Process. Control.*, **44** (2018), 288–306.
49. Z. Peng, G. Wang, H. Jiang, S. Meng, Research and improvement of ECG compression algorithm based on EZW, *Comput. Meth. Prog. Bio.*, **145** (2017), 157–166.
50. F. Wang, Q. Ma, W. Liu, S. Chang, novel ECG signal compression method using spindle convolutional auto-encoder, *Comput. Meth. Prog. Bio.*, **175** (2019), 139–150.

51. O. Yildirim, R. S. Tan, U. R. Acharya, An efficient compression of ECG signals using deep convolutional autoencoders, *Cognit. Syst. Res.*, **52** (2018), 198–211.
52. Research Resource for Complex Physiologic Signals (PhysioNet), Available online: <https://physionet.org/about/database/#restricted>.
53. A. L. Goldberger, L. A. N. Amaral, L. Glass, J. M. Hausdorff, P. C. Ivanov, PhysioBank, PhysioToolkit, and PhysioNet: components of a new research resource for complex physiologic signals, *Circulation*, **101** (2000), e215–e220.
54. M. B. Hossain, S. K. Bashar, A. J. Walkey, D. D. McManus, K. H. Chon, An accurate QRS complex and P wave detection in ECG signals using complete ensemble empirical mode decomposition with adaptive noise approach, *IEEE Access*, **7** (2019), 128869–128880.



AIMS Press

©2021 the Author(s), licensee AIMS Press. This is an open access article distributed under the terms of the Creative Commons Attribution License (<http://creativecommons.org/licenses/by/4.0>)